

Aggregation-induced emission and thermally activated delayed fluorescence of 2,6-diaminobenzophenones

Masaki Shimizu*, Masaki Nakatani & Kenta Nishimura

Faculty of Molecular Chemistry and Engineering, Kyoto Institute of Technology, Kyoto 606-8585, Japan

Received April 30, 2018; accepted June 5, 2018; published online July 13, 2018

Exploration of novel organic luminophores that exhibit thermally activated delayed fluorescence (TADF) in the aggregated state is very crucial for advance of delayed luminescence-based applications such as time-gated bio-sensing and temperature sensing. We report herein that synthesis, photophysical properties, molecular and crystal structures, and theoretical calculations of 2,6-bis(diarylamino)benzophenones. Absorption spectra in solution and calculations using density functional theory (DFT) method revealed that the optical excitation took place through intramolecular charge-transfer from one diarylamino moiety to an aroyl group. While the benzophenones did not luminesce in solution, the solids of the benzophenones emitted green light with moderate-to-good quantum yields. Thus, the benzophenones exhibit aggregation-induced emission. Based on the lifetime measurement, the green emission of the solids was found to include TADF. The emergence of the TADF is supported by the small energy gap between the excited singlet and triplet states, which was estimated by time-dependent DFT calculations. Thin films of poly(methyl methacrylate) doped by the benzophenones also showed green prompt and delayed fluorescence whose lifetimes were in the order of microseconds. Linear correlation between logarithm value of TADF lifetime and temperature was observed with the benzophenone in powder, suggesting that the benzophenones can serve as molecular thermometers workable under aqueous conditions.

donor-acceptor system, delayed fluorescence, temperature sensor

Citation: Shimizu M, Nakatani M, Nishimura K. Aggregation-induced emission and thermally activated delayed fluorescence of 2,6-diaminobenzophenones. *Sci China Chem*, 2018, 61, <https://doi.org/10.1007/s11426-018-9301-6>

1 Introduction

Organic luminophores that exhibit thermally activated delayed fluorescence (TADF) have drawn attention as emitters for organic light-emitting diodes (OLEDs) because internal quantum efficiency for TADF emitter-based OLEDs can, in principle, reach to 100% [1–4]. The long-lived luminescence is also beneficial for applications to time-gated bio-imaging and chemical sensing, which can eliminate the effects of background emission and scattered excitation light [5–8]. Since TADF is a radiative decay process from the lowest singlet excited state (S_1) generated from the lowest triplet

excited state (T_1) by reverse intersystem crossing, a small energy gap between S_1 and T_1 (ΔE_{ST}) is essential for realizing TADF. Organic luminophores including TADF-emissive ones mostly experience severe concentration quenching of luminescence in the aggregated state [9,10]. Hence, TADF can be generally attained when the luminophore is dispersed in a host matrix, whereas is difficult to observe in neat solids [11–14]. However, efficient TADF in neat solid can allow us to develop nondoped TADF-based OLEDs, which have several advantages over doped OLEDs. As bio-imaging and -sensing are usually carried out in aqueous conditions where organic luminophores readily form aggregates, the realization of TADF in neat solid is also desired in view of such target-detecting applications in water. Several organic lu-

*Corresponding author (email: mshimizu@kit.ac.jp)

minophores that exhibit aggregation-induced emission (AIE) of TADF are developed, but the repertoire of the molecular structures is quite limited [15–23]. Therefore, it is important to explore a novel class of AIE-active TADF emitters and disclose their photophysical properties.

During our studies on the development of donor and acceptor-substituted organic luminophores that exhibit efficient solid-state emission [24–33], we found that powder of 2-(diarylamino)isophthalic acid diesters that can be classified as 1,3-bis(acceptor)-2-donor-substituted benzenes (**ADA**), showed aggregation-induced fluorescence, and the thin film of poly(methyl methacrylate) (PMMA) doped with the diesters exhibited delayed fluorescence (**Scheme 1**) [34]. The emergence of delayed fluorescence with the isophthalates is ascribed to the largely twisted conformation and the intramolecular charge-transfer (ICT) from the diarylamino group to the isophthalate moiety, both of which are originated from the sandwiching layout of a donor with two acceptors on a benzene core. Then, we became interested in 1,3-bis(donor)-2-acceptor-substituted benzenes (**DAD**), which can be regarded as an electronically reversed structure of 2-(diarylamino)isophthalic acid diester, as novel luminophores exhibiting delayed fluorescence (**Scheme 1**). We report herein the synthesis, photophysical properties, molecular and crystal structures, and theoretical calculations of 2,6-bis(diarylamino)benzophenones **1** as one example of **DAD**-type luminophores.

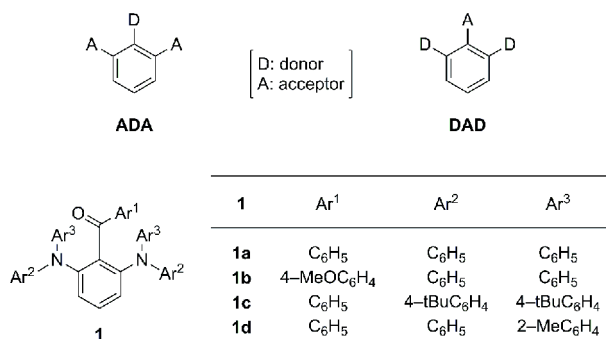
2 Experimental

To a 250 mL Schlenk flask charged with tetrahydrofuran (THF) (30 mL) and 1,3-dibromobenzene (1.2 mL, 10 mmol) was added lithium diisopropylamide (1.4 M in THF, 7.6 mL, 11 mmol) slowly at $-78\text{ }^{\circ}\text{C}$. The solution was stirred at $-78\text{ }^{\circ}\text{C}$ for 1 h. Benzaldehyde (1.0 mL, 10 mmol) was slowly added to the flask at $-78\text{ }^{\circ}\text{C}$, and the resulting mixture was warmed to room temperature and stirred for 17 h before quenching with sat. aq. NH_4Cl (30 mL). The aqueous layer was extracted with EtOAc (50 mL) and the combined or-

ganic layer was washed with water, dried over anhydrous MgSO_4 , and concentrated in vacuo. The crude product, KMnO_4 (1.4 g, 8.8 mmol), *t*-BuOH (30 mL), and water (30 mL) were charged into a 300 mL three-necked flask, and the mixture was stirred at $60\text{ }^{\circ}\text{C}$ for 12 h. The resulting mixture was filtered through a pad of Celite, and the filtrate was extracted with EtOAc (50 mL). The combined organic layer was washed with water (three times), dried over anhydrous MgSO_4 , and concentrated in vacuo. The crude product was purified with column chromatography on silica gel (eluent: hexane/EtOAc, 10:1) and then recrystallization from CH_2Cl_2 /hexane to give 2,6-dibromobenzophenone (2.3 g, 6.8 mmol, 68%) as colorless solid. An 80 mL Schlenk flask was charged with 2,6-dibromobenzophenone (0.80 g, 2.3 mmol), $\text{Pd}_2(\text{dba})_3$ (84 mg, 91 μmol , 4 mol%), 2-dicyclohexylphosphino-2',4',6'-triisopropylbiphenyl (XPhos; 0.18 g, 0.38 mmol, 16 mol%), and K_2CO_3 (1.3 g, 9.2 mmol). The flask was evacuated and filled with argon. This evacuation-argon filling operation was repeated twice. To the flask was added toluene (8 mL) and aniline (0.44 mL, 4.8 mmol). The solution was stirred at $100\text{ }^{\circ}\text{C}$ for 21 h. The resulting solution was diluted with EtOAc (30 mL), filtered through a pad of Celite, and concentrated in vacuo. The crude product was purified by silica gel column chromatography (eluent: hexane/EtOAc, 10:1) to give 2,6-bis(phenylamino)benzophenone (0.70 g, 0.19 mmol, 83%) as orange solid. To an 80 mL Schlenk flask was added 2,6-bis(phenylamino)benzophenone (0.36 g, 1.0 mmol), K_2CO_3 (0.56 g, 4.0 mmol), and Cu (19 mg, 0.30 mmol, 30 mol%). The flask was evacuated and filled with argon. This evacuation-argon filling operation was repeated twice. Iodobenzene (5 mL) was added to the flask. The resulting mixture was stirred at $200\text{ }^{\circ}\text{C}$ for 3 d. The mixture was diluted with CH_2Cl_2 (30 mL) and filtered through a pad of Celite, and concentrated in vacuo. The crude product was purified by silica gel column chromatography (eluent: hexane/EtOAc, 10:1) and then recrystallization from CH_2Cl_2 /hexane (three times) to give **1a** (0.48 g, 0.93 mmol, 93%) as yellow-green solid.

1a: $T_m=124\text{ }^{\circ}\text{C}$, $T_d=286\text{ }^{\circ}\text{C}$. TLC: $R_f=0.42$ (hexane/EtOAc, 10:1). ^1H NMR (CDCl_3 , 400 MHz): δ 6.80–6.83 (m, 12H), 7.00–7.07 (m, 10H), 7.14 (d, $J=8.0$ Hz, 2H), 7.19–7.24 (m, 3H), 7.38 (t, $J=8.0$ Hz, 1H); ^{13}C NMR (CDCl_3 , 100 MHz): δ 122.3, 123.4, 125.5, 127.0, 128.7, 129.0, 130.9, 132.2, 136.4, 136.5, 147.4, 147.6, 194.0. IR (neat): 3055, 1658, 1581, 1487, 1444, 1249, 1074, 916, 748, 692 cm^{-1} . HRMS (FAB): $[\text{M}]^+$ calcd for $[\text{C}_{37}\text{H}_{28}\text{N}_2\text{O}]$: 516.2202, found: 516.2209.

1b: Isolated in 86% yield. $T_m=136\text{ }^{\circ}\text{C}$, $T_d=294\text{ }^{\circ}\text{C}$. TLC: $R_f=0.36$ (hexane/EtOAc 10:1). ^1H NMR (CDCl_3 , 400 MHz): δ 3.71 (s, 3H), 6.49 (d, $J=8.4$ Hz, 2H), 6.79–6.83 (m, 12H), 7.03–7.07 (m, 8H), 7.14 (d, $J=8.0$ Hz, 2H), 7.19 (d, $J=8.4$ Hz, 2H), 7.35 (t, $J=8.0$ Hz, 1H); ^{13}C NMR (CDCl_3 , 100 MHz): δ 55.1, 112.2, 122.1, 123.3, 125.6, 128.6, 130.0,



Scheme 1 Molecular structures of 2,6-diaminobenzophenones **1**.

130.6, 131.2, 136.8, 147.4, 162.5, 192.5. IR (neat): 3003, 1654, 1587, 1483, 1442, 1315, 1247, 1166, 1022, 923, 750, 688 cm^{-1} . HRMS (FAB): $[M]^+$ calcd for $[\text{C}_{38}\text{H}_{30}\text{N}_2\text{O}_2]$: 546.2307, found: 546.2307.

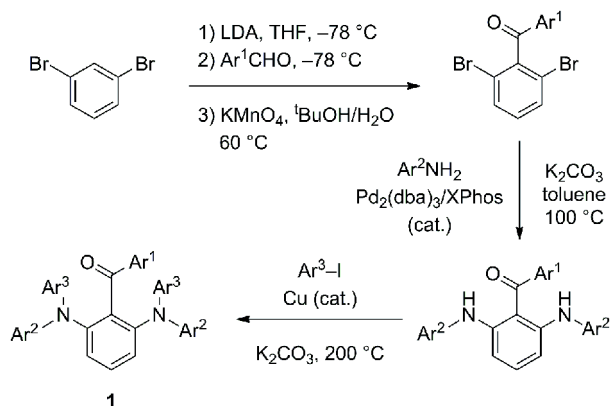
1c: Isolated in 75% yield. T_m (dec)=330 °C. TLC: R_f =0.75 (hexane/EtOAc, 10:1). ^1H NMR (CDCl_3 , 400 MHz): δ 1.19 (s, 36H), 6.72 (d, J =8.4 Hz, 8H), 6.90 (t, J =7.6 Hz, 2H), 7.02 (d, J =8.4 Hz, 8H), 7.09–7.12 (m, 5H), 7.34 (t, J =7.6 Hz, 1H); ^{13}C NMR (CDCl_3 , 100 MHz): δ 31.4, 34.0, 122.8, 125.3, 125.4, 126.7, 129.0, 130.6, 131.8, 136.3, 136.4, 144.6, 145.0, 147.8, 194.4. IR (neat): 2955, 1620, 1565, 1506, 1456, 1363, 1263, 1192, 1120, 920, 825, 688 cm^{-1} . HRMS (FAB): $[M]^+$ calcd for $[\text{C}_{53}\text{H}_{60}\text{N}_2\text{O}]$: 740.4706, found: 740.4700.

1d: Isolated in 70% yield. T_m =149 °C, T_d =303 °C. TLC: R_f =0.62 (hexane/EtOAc, 10:1). ^1H NMR (CDCl_3 , 400 MHz): δ 1.39 (s, 6H), 6.74–6.84 (m, 12H), 6.96 (t, J =8.0 Hz, 2H), 7.04 (d, J =8.0 Hz, 4H), 7.09 (t, J =8.0 Hz, 4H), 7.20 (t, J =8.0 Hz, 1H), 7.25–7.31 (m, 3H); ^{13}C NMR (CDCl_3 , 100 MHz): δ 18.3, 121.3, 121.6, 123.5, 124.8, 126.5, 127.1, 127.9, 128.7, 129.0, 129.8, 131.2, 132.1, 134.4, 134.9, 135.7, 144.6, 148.2, 148.6, 193.8. IR (neat): 3016, 1664, 1568, 1485, 1446, 1226, 1114, 1033, 925, 752, 692 cm^{-1} . HRMS (FAB): $[M]^+$ calcd for $[\text{C}_{39}\text{H}_{32}\text{N}_2\text{O}]$: 544.2515, found: 544.2521.

3 Results and discussion

3.1 Synthesis of 2,6-diaminobenzophenones **1**

Diaminobenzophenones **1** were synthesized from 1,3-dibromobenzene (Scheme 2). Carbonyl addition of 2,6-dibromophenyllithium, generated from the dibromobenzene with LDA, to Ar^1CHO gave the corresponding diarylmethanols, which was oxidized with KMnO_4 to afford 2,6-dibromophenyl ketones. Pd-catalyzed amination of the dibrominated ketones with anilines Ar^2NH_2 and subsequent coupling with aryl iodides $\text{Ar}^3\text{-I}$ with the aid of copper catalyst provided **1** in good-to-high yields.



Scheme 2 Synthesis of **1**.

3.2 Photophysical properties

3.2.1 UV-visible absorption properties in solution

UV-visible absorption data and spectra of **1** in a 2:1:1 mixed solution of diethyl ether, toluene, and ethanol (ETE) are shown in Table 1 and Figure 1, respectively. The weak and broad bands were observed with absorption maxima at 365–378 nm. The absorption maxima of **1c** possessing (4-*t*-Bu C_6H_4) $_2\text{N}$, more electron-donating group than Ph_2N , and **1b** bearing 4-MeOC $_6\text{H}_4\text{CO}$, less electron-accepting group than PhCO , were red- and blue-shifted, respectively, compared with that of **1a**. Based on the experimental results and theoretical calculations using density functional theory (DFT), the weak bands were ascribed to ICT from one diarylamino moiety to the aryl group (see 3.4 Theoretical calculations). The hypochromic shift of absorption maximum of **1d** with respect to **1a** implied that the effective conjugation length of **1d** was shorter than that of **1a**. This may be reasonable by assuming that the conformation of diarylamino groups of **1d** is more twisted than those of **1a** due to the sterically demanding *ortho*-tolyl groups.

3.2.2 Aggregation-induced emission

All of **1** in solution were non-luminescent at room temperature. The luminescence quenching was probably ascribed to intramolecular motions possible in solution and collision with solvent molecules at room temperature, which led to the loss of the excited energy. Then, AIE behavior was examined by adding water to a THF solution of **1b** (Figure 2. For **1a**, **1c**, and **1d**, see Supporting information online). The mixed solutions of THF and water were non-emissive when

Table 1 Absorption data of **1** in a 2:1:1 mixed solution (10^{-5} M) of diethyl ether, toluene, and ethanol (ETE)

1	λ_{abs} (nm)	ϵ ($\text{M}^{-1} \text{cm}^{-1}$)
1a	373	2200
1b	365	3100
1c	378	2200
1d	365	6000

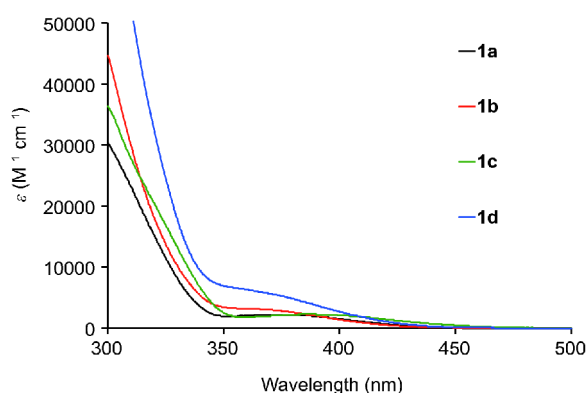


Figure 1 Absorption spectra of **1** in ETE (10^{-5} M) (color online).

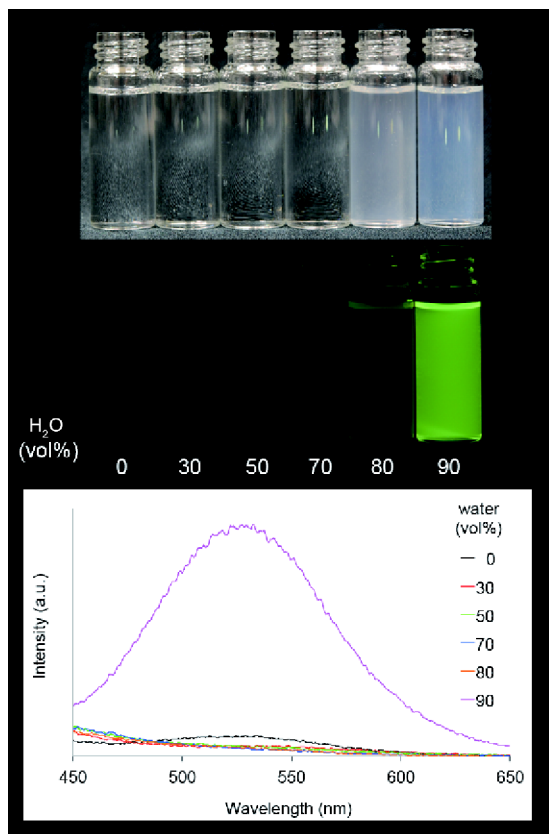


Figure 2 Optical (upper line) and luminescent (lower line) images and fluorescence spectra of **1b** in THF/H₂O (color online).

the water fraction was less than 90%. In case that the water fraction reached to 90%, the solution became green-luminescent. As **1b** was insoluble in water, the high water content in the mixed solution forced **1b** to form aggregates in which intramolecular motions resulting in non-radiative decay was suppressed. Hence, **1** was confirmed to exhibit AIE [35,36].

3.2.3 Photoluminescence properties in the solid state

As the aggregates of **1** showed luminescence, we next investigated the photoluminescence of **1** in the solid state at 298 K in air. The data and spectra are shown in Table 2 and Figure 3, respectively. Each solid emitted green light with emission maxima at 489–500 nm with moderate-to-good quantum yields of 0.36–0.58. The luminescence lifetime measurements revealed that the green emission included two

Table 2 Photoluminescence data of **1** in the solid state at 298 K in air^{a)}

1	λ_{em} (nm)	Φ	τ_1 (ns)	τ_2 (μ s)
1a	500	0.58	3.0	4.4
1b	496	0.55	3.6	3.3
1c	498	0.41	5.4	7.9
1d	489	0.36	0.6	1.8

a) Excitation was affected by UV irradiation at 350 nm for **1a**, **1b**, and **1d**, and 360 nm for **1c**.

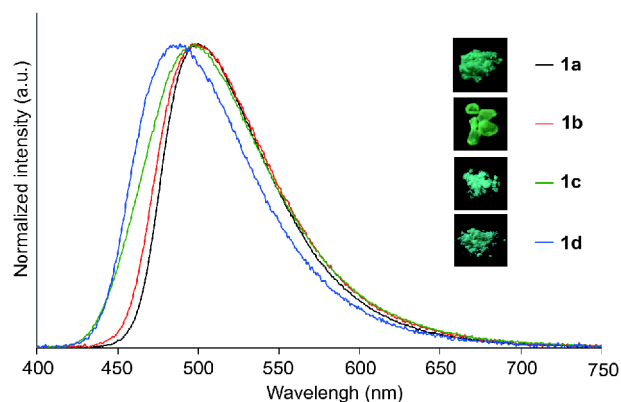


Figure 3 Fluorescence spectra of **1** in the solid state at 298 K in air (color online).

decay rates: one was in the order of nanoseconds and the other was in the order of microseconds. Hence, **1** in the solid state was found to exhibit dual emission of prompt and delayed fluorescence.

3.2.4 Photoluminescence properties in solution at 77 K

A solution of **1** in ETE at 77 K exhibited green emission at 485–509 nm with good-to-excellent quantum yields of 0.56–0.92 (Table 3 and Figure 4). The emission maxima of **1b** and **1c** were hypsochromically and bathochromically shifted, respectively, compared with **1a**, which corresponded to the trend of their absorption maxima and ICT character. The lifetimes of long-lived emission at 77 K were in the order of milliseconds, which were much longer than those of the solids at 298 K, and the long-lived emission is assignable as

Table 3 Photoluminescence data of **1** in ETE at 77 K^{a)}

1	λ_{em} (nm)	Φ	τ_1 (ns)	τ_2 (ms)
1a	504	0.76	2.8	10.0
1b	492	0.92	4.4	21.2
1c	509	0.84	3.8	7.8
1d	485	0.56	2.8	18.7

a) Excitation was affected by UV irradiation at 350 nm for **1a**, **1b**, and **1d**, and 360 nm for **1c**.

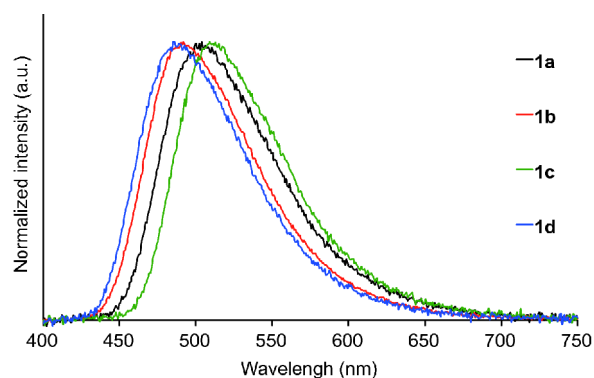


Figure 4 Fluorescence spectra of **1** in ETE at 77 K (color online).

phosphorescence. Although the quantum yields at 77 K were much higher than those of solids at 298 K, no discernible phosphorescence band was observed in the spectra shown in Figure 4, suggesting that the values of ΔE_{ST} were very small.

3.2.5 Photoluminescence properties in PMMA film

Table 4 summarizes photoluminescence data of **1** dispersed in PMMA film at 298 K under vacuum. As shown in Figure 5, the emission maxima and spectral shape were almost similar, and each spectrum were red-shifted compared with those of the solids at 298 K and in ETE at 77 K, although the reason is unclear. Short and long lifetimes in the order of nano- and microseconds, respectively, were observed with the PMMA films as with the solids at 298 K, indicating that the green emission of the films also consisted of prompt and delayed fluorescence. In air, the quantum yields of the films slightly lowered compared with those under vacuum. The decrease of the luminescence quantum yields in air should be attributed to the quenching of the triplet excited state by molecular oxygen, and hence the values of the decrease, in principle, correspond to the quantum yields of delayed fluorescence. However, even in air, the emission components whose lifetimes were in the order of microseconds were still observed with all of **1**. This means that un-quenched triplet species remain in the PMMA films in air, and the quantum yields for delayed fluorescence cannot be simply estimated from the difference of the quantum yields ($\Delta\Phi$) between under vacuum (Φ_{vacuum}) and in air (Φ_{air}).

Table 4 Photoluminescence data of **1** dispersed in PMMA film at 298 K under vacuum^{a)}

1	λ_{em} (nm)	Φ_{vacuum}	τ_1 (ns)	τ_2 (μs)	$\Delta\Phi^{\text{b)}$
1a	523	0.30	9.7	2.7	0.04
1b	531	0.34	3.8	4.5	0.04
1c	522	0.39	5.1	3.6	0.16
1d	531	0.30	4.1	3.2	0.02

a) Excitation was affected by UV irradiation at 350 nm for **1a**, **1b**, and **1d**, and 360 nm for **1c**. b) $\Delta\Phi = \Phi_{\text{vacuum}} - \Phi_{\text{air}}$.

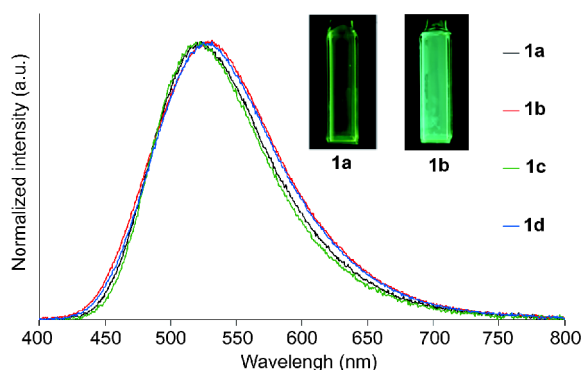


Figure 5 Fluorescence spectra and luminescent images of **1** in PMMA film at 298 K under vacuum (color online).

3.3 Molecular and crystal structures of **1b**

Recrystallization of **1b** from hexane/ CH_2Cl_2 solution gave its single crystals suitable for X-ray diffraction analysis [37]. The carbonyl group is twisted with respect to the diamino-benzene ring by 55.86° to diminish the steric repulsion against the two NPh_2 groups (Figure 6(a)). Each bond angle around the nitrogen atoms is almost 120° , indicating that the nitrogen atoms are sp^2 hybridized. As shown in Figure 6(b), a carbonyl moiety and one phenyl group of a Ph_2N moiety form intramolecular π - π stacking with atomic distances of 3.009–3.383 Å. Crystal packing diagram demonstrates that each molecule of **1b** (Figure 7) is positioned far from each other and there is no intermolecular π - π stacking resulting in the loss of the excited energy, presumably due to the distorted molecular conformation, which is essential for the efficient solid-state emission.

3.4 Theoretical calculations

Molecular orbital calculations of **1a–1c** were carried out by DFT method at the B3LYP/cc-pVDZ//B3LYP/cc-pVDZ level using the Gaussian 09 package (Table 5) [38]. The molecular structures were optimized using initial structures based on the molecular structure of **1b** determined by X-ray analysis. Each highest occupied molecular orbital (HOMO)

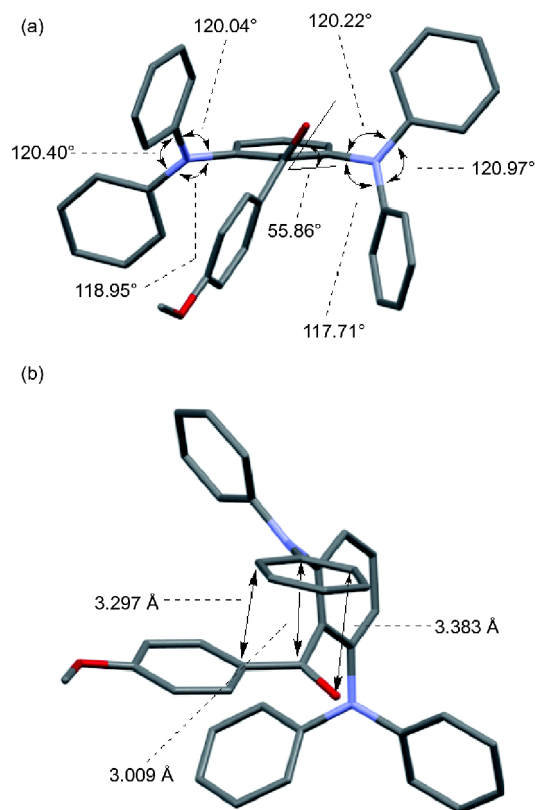


Figure 6 Molecular structure of **1b**. (a) Side view and (b) top view (color online).

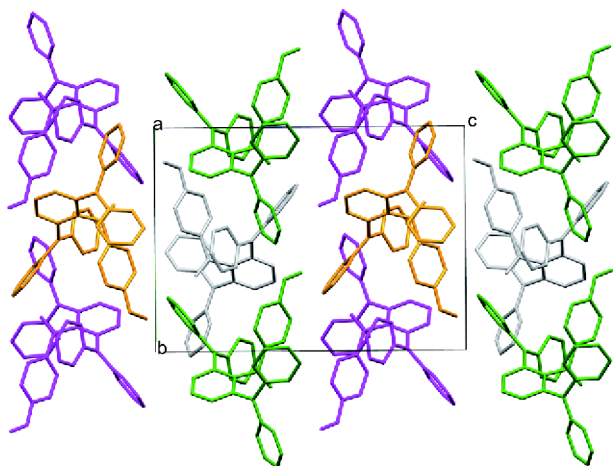


Figure 7 Crystal packing diagram of **1b** (a view from a axis). Each molecule is color-coded based on symmetry operations (color online).

Table 5 Calculated energies of LUMO, HOMO, S_1 , and T_1 and their energy gaps of **1a–1c**^{a)}

	1	1a	1b	1c
E_{LUMO} (eV)		−1.74	−1.52	−1.67
E_{HOMO} (eV)		−5.16	−5.10	−4.98
ΔE_{LH} (eV) ^{b)}		3.42	3.58	3.31
$\frac{\Delta E_{\text{LH}}}{\lambda_{\text{abs}}}$ (nm) ^{b)}		363/373	347/365	375/388
E_{S_1} (eV)		2.755	2.916	2.650
E_{T_1} (eV)		2.671	2.794	2.575
$\Delta E_{\text{S}_1\text{T}_1}$ (eV) ^{c)}		0.084	0.122	0.075

a) Calculated at the B3LYP/cc-pVDZ//B3LYP/cc-pVDZ level. b) $\Delta E_{\text{LH}} = E_{\text{LUMO}} - E_{\text{HOMO}}$. c) $\Delta E_{\text{S}_1\text{T}_1} = E_{\text{S}_1} - E_{\text{T}_1}$.

is localized over one Ar_2N moiety that does not form intramolecular π - π stacking and a central benzene ring (Figure 8). It should be noted that another Ar_2N moiety does not participate in the HOMO. The lowest unoccupied molecular orbitals (LUMOs) are developed over a central benzene ring and an aroyl group. Thus, the HOMOs and LUMOs are separated with little overlap on the central benzene ring. Time-dependent (TD) DFT calculations of the optimized structures indicate that the lowest energy transitions are assignable to the transition from the HOMOs to LUMOs. The calculated larger and smaller HOMO-LUMO energy gaps (ΔE_{LH}) of **1b** and **1c**, respectively, with respect to **1a** are matched with the trend of their absorption maxima. Hence, the optical excitation, i.e., absorption, of **1** is concluded to involve ICT from one Ar_2N moiety to an aroyl group. The calculated values of $\Delta E_{\text{S}_1\text{T}_1}$ are 0.075 to 0.122, which are small enough to facilitate RISC and emergence of TADF. These calculations allow us to confirm the validity of the ICT excitation mechanism and molecular orbital calculations using (TD)-DFT method are reliable for elucidating the electronic

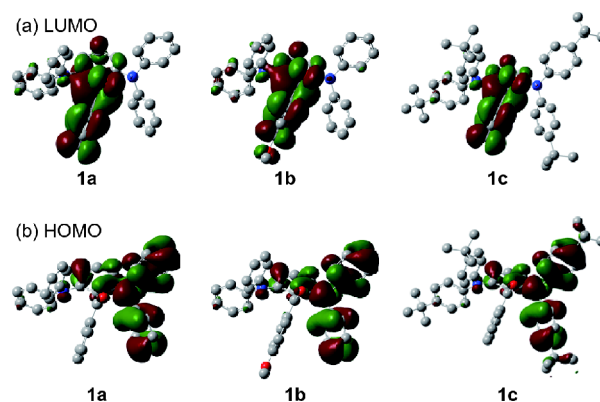


Figure 8 LUMO and HOMO drawings of **1a–1c**.

structure of **1**.

3.5 Applications to temperature sensing

Temperature sensing that uses organic luminophores has attracted broad attention in various fields because molecular thermometer can measure temperature in a very small space such as a living cell and a microfluidic channel [39–45]. In view that the excited triplet states are very sensitive to temperature, we measured the lifetime of **1b** in powder at temperatures ranging from -80 to 80 °C. Figure 9 shows the dependence of logarithm value of delayed fluorescence lifetime on temperature. The relationship can be expressed as negative direct function with a coefficient of determination being 0.988. The finding that the aggregated **1b** can sense temperature with high accuracy opens the possibility of **1** as a molecular thermometer for measurement of the temperature of living cells where organic luminophores definitely form aggregates due to the aqueous conditions.

4 Conclusions

We have demonstrated that 2,6-bis(diarylamino)benzo phe-

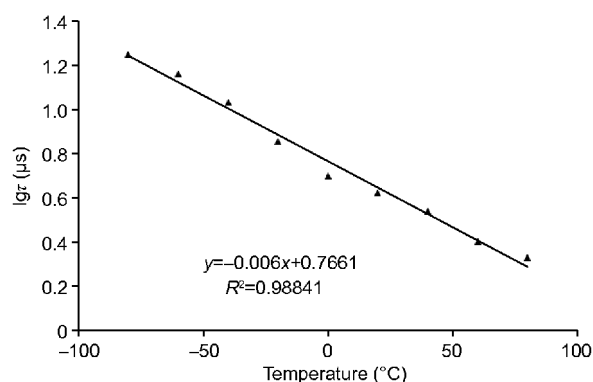


Figure 9 Temperature dependence of the DF lifetime of **1b**.

nones serve as novel luminophores that exhibit AIE of prompt and delayed fluorescence. The delayed fluorescence is also observed when the benzophenones are dispersed in PMMA films. The absorption process occurred via intramolecular charge-transfer from one diarylamino moiety to an aroyl group. In other words, the second amino moiety does not be involved as a donor in the photophysical processes. This finding may lead to new guiding principle for the molecular design of organic luminophores that exhibit aggregation-induced delayed fluorescence. Further researches on the design and development of novel luminophores with AIE character are under way.

Acknowledgements This work was supported by Grants-in-Aid for JSPS KAKENHI (15H03795), MEXT KAKENHI 15K13671, the Nagase Science and Technology Foundation, and the Ogasawara Foundation for the Promotion of Science and Engineering.

Conflict of interest The authors declare that they have no conflict of interest.

Supporting information The supporting information is available online at <http://chem.scichina.com> and <http://link.springer.com/journal/11426>. The supporting materials are published as submitted, without typesetting or editing. The responsibility for scientific accuracy and content remains entirely with the authors.

- Uoyama H, Goushi K, Shizu K, Nomura H, Adachi C. *Nature*, 2012, 492: 234–238
- Nakanotani H, Higuchi T, Furukawa T, Masui K, Morimoto K, Numata M, Tanaka H, Sagara Y, Yasuda T, Adachi C. *Nat Commun*, 2014, 5: 4016
- Zhang Q, Li B, Huang S, Nomura H, Tanaka H, Adachi C. *Nat Photon*, 2014, 8: 326–332
- Kaji H, Suzuki H, Fukushima T, Shizu K, Suzuki K, Kubo S, Komino T, Oiwa H, Suzuki F, Wakamiya A, Murata Y, Adachi C. *Nat Commun*, 2015, 6: 8476
- Marriott G, Clegg RM, Arndt-Jovin DJ, Jovin TM. *Biophys J*, 1991, 60: 1374–1387
- Carretero AS, Castillo AS, Gutiérrez AF. *Crit Rev Anal Chem*, 2005, 35: 3–14
- Suhling K, French PMW, Phillips D. *Photochem Photobiol Sci*, 2005, 4: 13–22
- Xiong X, Song F, Wang J, Zhang Y, Xue Y, Sun L, Jiang N, Gao P, Tian L, Peng X. *J Am Chem Soc*, 2014, 136: 9590–9597
- Shimizu M, Hiyama T. *Chem Asian J*, 2010, 5: 1516–1531
- Li Q, Li Z. *Adv Sci*, 2017, 4: 1600484
- Wong MY, Zysman-Colman E. *Adv Mater*, 2017, 29: 1605444
- Im Y, Kim M, Cho YJ, Seo JA, Yook KS, Lee JY. *Chem Mater*, 2017, 29: 1946–1963
- Yang Z, Mao Z, Xie Z, Zhang Y, Liu S, Zhao J, Xu J, Chi Z, Aldred MP. *Chem Soc Rev*, 2017, 46: 915–1016
- Tao Y, Yuan K, Chen T, Xu P, Li H, Chen R, Zheng C, Zhang L, Huang W. *Adv Mater*, 2014, 26: 7931–7958
- Chen B, Sun X, Evans RE, Zhou R, Demas JN, Trindle CO, Zhang G. *J Phys Chem A*, 2015, 119: 8854–8859
- Xu S, Liu T, Mu Y, Wang YF, Chi Z, Lo CC, Liu S, Zhang Y, Lien A, Xu J. *Angew Chem Int Ed*, 2015, 54: 874–878
- Xie Z, Chen C, Xu S, Li J, Zhang Y, Liu S, Xu J, Chi Z. *Angew Chem Int Ed*, 2015, 54: 7181–7184
- Gan S, Luo W, He B, Chen L, Nie H, Hu R, Qin A, Zhao Z, Tang BZ. *J Mater Chem C*, 2016, 4: 3705–3708
- Furue R, Nishimoto T, Park IS, Lee J, Yasuda T. *Angew Chem Int Ed*, 2016, 55: 7171–7175
- Tsujimoto H, Ha DG, Markopoulos G, Chae HS, Baldo MA, Swager TM. *J Am Chem Soc*, 2017, 139: 4894–4900
- Guo J, Li X-L, Nie H, Luo W, Gan S, Hu S, Hu R, Qin A, Zhao Z, Su S-J, Tang BZ. *Adv Funct Mater*, 2017, 1606458
- Wang T, Wu Z, Sun W, Jin S, Zhang X, Zhou C, Jiang J, Luo Y, Zhang G. *J Phys Chem A*, 2017, 121: 7183–7190
- Guo J, Li XL, Nie H, Luo W, Hu R, Qin A, Zhao Z, Su SJ, Tang BZ. *Chem Mater*, 2017, 29: 3623–3631
- Shimizu M, Takeda Y, Higashi M, Hiyama T. *Angew Chem Int Ed*, 2009, 48: 3653–3656
- Shimizu M, Asai Y, Takeda Y, Yamatani A, Hiyama T. *Tetrahedron Lett*, 2011, 52: 4084–4089
- Shimizu M, Takeda Y, Higashi M, Hiyama T. *Chem Asian J*, 2011, 6: 2536–2544
- Shimizu M, Kaki R, Takeda Y, Hiyama T, Nagai N, Yamagishi H, Furutani H. *Angew Chem Int Ed*, 2012, 51: 4095–4099
- Shimizu M, Tamagawa T. *Eur J Org Chem*, 2015, 2015: 291–295
- Shimizu M, Fukui H, Natakani M, Sakaguchi H. *Eur J Org Chem*, 2016, 2016: 5950–5956
- Shimizu M, Fukui H, Shigitani R. *Jnl Chin Chem Soc*, 2016, 63: 317–322
- Shimizu M, Kimura A, Sakaguchi H. *Eur J Org Chem*, 2016, 2016: 467–473
- Shimizu M, Shigitani R, Nakatani M, Kuwabara K, Miyake Y, Tajima K, Sakai H, Hasobe T. *J Phys Chem C*, 2016, 120: 11631–11639
- Shimizu M, Kinoshita T, Shigitani R, Miyake Y, Tajima K. *Mater Chem Front*, 2018, 2: 347–354
- Shimizu M, Nakatani M. *Eur J Org Chem*, 2017, 2017: 4695–4702
- Mei J, Leung NLC, Kwok RTK, Lam JWY, Tang BZ. *Chem Rev*, 2015, 115: 11718–11940
- Mei J, Hong Y, Lam JWY, Qin A, Tang Y, Tang BZ. *Adv Mater*, 2014, 26: 5429–5479
- CCDC 1840378 (for **1b**) contains the supplementary crystallographic data for this paper. These data can be obtained free of charge from The Cambridge Crystallographic Data Centre
- Frisch MJ, Trucks GW, Schlegel HB, Scuseria GE, Robb MA, Cheeseman JR, Scalmani G, Barone V, Mennucci B, Petersson GA, Nakatsuji H, Caricato M, Li X, Hratchian HP, Izmaylov AF, Bloino J, Zheng G, Sonnenberg JL, Hada M, Ehara M, Toyota K, Fukuda R, Hasegawa J, Ishida M, Nakajima T, Honda Y, Kitao O, Nakai H, Vreven T, Montgomery JA Jr, Peralta JE, Ogliaro F, Bearpark M, Heyd JJ, Brothers E, Kudin KN, Staroverov VN, Kobayashi R, Normand J, Raghavachari K, Rendell A, Burant JC, Iyengar SS, Tomasi J, Cossi M, Rega N, Millam JM, Klene M, Knox JE, Cross JB, Bakken V, Adamo C, Jaramillo J, Gomperts R, Stratmann RE, Yazyev O, Austin AJ, Cammi R, Pomelli C, Ochterski JW, Martin RL, Morokuma K, Zakrzewski VG, Voth GA, Salvador P, Dannenberg JJ, Dapprich S, Daniels AD, Farkas Ö, Foresman JB, Ortiz JV, Cioslowski J, Fox DJ. Gaussian 09, revision D.01. Wallingford: Gaussian, Inc., 2013
- Schrum KF, Williams AM, Haerther SA, Ben-Amotz D. *Anal Chem*, 1994, 66: 2788–2790
- Fister JC, Rank D, Harris JM. *Anal Chem*, 1995, 67: 4269–4275
- Uchiyama S, Prasanna de Silva A, Iwai K. *J Chem Educ*, 2006, 83: 720–727
- Brites CDS, Lima PP, Silva NJO, Millán A, Amaral VS, Palacio F, Carlos LD. *Nanoscale*, 2012, 4: 4799–4829
- McLaurin EJ, Bradshaw LR, Gamelin DR. *Chem Mater*, 2013, 25: 1283–1292
- Bai T, Gu N. *Small*, 2016, 12: 4590–4610
- Uchiyama S, Gota C, Tsuji T, Inada N. *Chem Commun*, 2017, 53: 10976–10992